ACS OMEGA

http://pubs.acs.org/journal/acsodf

Article

Graphene Nanoplatelet/Multiwalled Carbon Nanotube/Polypyrrole Hybrid Fillers in Polyurethane Nanohybrids with 3D Conductive Networks for EMI Shielding

Chih-Lung Lin, Jia-Wun Li, Yan-Feng Chen, Jian-Xun Chen, Chih-Chia Cheng, and Chih-Wei Chiu*

Cite This: *ACS Omega* 2022, 7, 45697−45707

Read Online

ACCESS | Metrics & More | Article Recommendations | Supporting Information

ABSTRACT: This work reports the preparation of graphene nanoplatelet (GNP)/multiwalled carbon nanotube (MWCNT)/polypyrrole (PPy) hybrid fillers via in situ chemical oxidative polymerization with the addition of a cationic surfactant, hexadecyltrimethylammonium bromide. These hybrid fillers were incorporated into polyurethane (PU) to prepare GNP/MWCNT/PPy/PU nanohybrids. The electrical conductivity of the nanohybrids was synergistically enhanced by the high conductivity of the hybrid fillers. Furthermore, the electromagnetic interference (EMI) shielding effectiveness (SE) was greatly increased by interfacial polarization between the GNPs, MWCNTs, PPy, and PU. The optimal formulation for the preparation of GNP/MWCNT/PPy three-dimensional (3D) nanostructures was determined by optimization experiments. Using this formulation, we successfully prepared GNP/PPy nanolayers (two-dimensional) that are extensively covered by MWCNT/PPy nanowires (one-dimensional), which interconnect to form GNP/MWCNT/PPy 3D nanostructures. When incorporated into a PU matrix to form a nanohybrid, these 3D nanostructures form a continuous network of conductive GNP−PPy−CNT−PPy−GNP paths. The EMI SE of the nanohybrid is 35−40 dB at 30−1800 MHz, which is sufficient to shield over 99.9% of electromagnetic waves. Therefore, this EMI shielding material has excellent prospects for commercial use. In summary, a nanohybrid with excellent EMI SE performance was prepared using a facile and scalable method and was shown to have great commercial potential.

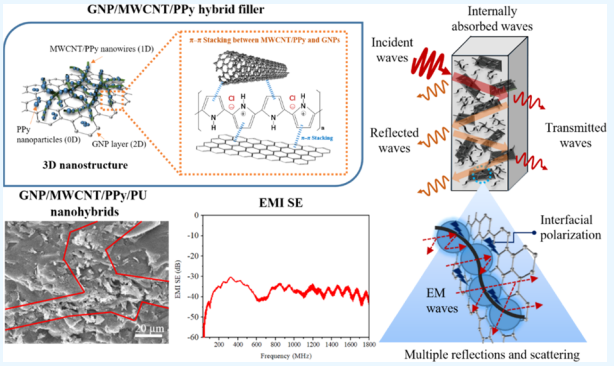

1. INTRODUCTION

With the rapid development of electronic devices, these devices are finding applications in various fields, including telecommunications, science, industry, the military, and daily life. However, electromagnetic interference (EMI) can reduce or degrade the performance of electronic devices and have detrimental effects on human health. Therefore, researchers have developed EMI shielding materials that attenuate the most severe forms of electromagnetic radiation.[1−3] Although metals are excellent EMI shielding materials, they are susceptible to corrosion, difficult to form, and heavy; thus, they are unsuitable for many applications.[4] Lightness and flexibility are important technical requirements for high-performance EMI shielding materials, as they are essential for flexible electronics, aircraft, and wearable devices.[5] For this reason, EMI shielding polymer nanocomposites are often prepared using conductive filler materials with excellent dielectric and magnetic properties, such as carbon black,[6] carbon nanotubes (CNTs),[7] graphene,[8,9] metal nanoparticles,[10] conductive polymers,[11] and core−shell composites.[12] Many zero- (0D), one- (1D), two- (2D), and three-dimensional (3D) materials have also been studied and combined to create conductive filler materials.[13−17] Furthermore, it has been shown that the EMI shielding efficiency (SE) of a filler material is also significantly affected by its structural characteristics.

The conductivity of polymer nanocomposites depends strongly on the uniform dispersion of a hybrid filler in the polymer matrix. The dispersed hybrid filler can form conduction pathways in the polymer matrix, which can contribute to the EMI SE.[18] One-dimensional CNTs and two-dimensional graphene are outstanding hybrid filler materials, as they have high aspect ratios and excellent mechanical and electrical properties.[19,20] Therefore, many researchers have attempted to combine these materials to form highly electrically conductive networks in a polymer matrix. Researchers have prepared 3D hybrid fillers by mixing CNTs with graphene nanoplatelets (GNPs), where their $\pi-\pi$ interactions were exploited to inhibit aggregation and improve

Received: October 13, 2022
Accepted: November 25, 2022
Published: December 5, 2022

morphological dispersion. The conductivity was also enhanced by maximizing the synergistic electron transfer effect between CNTs and graphene.[21,22] High-performance polymer/CNT composites have recently found widespread use in numerous applications, including sensors, supercapacitors, and water purifiers. Conductive polymers, in particular polypyrrole (PPy), are especially interesting because of their high conductivity, biocompatibility, low cost, and ease of synthesis.[23−25] However, PPy is mechanically weak, susceptible to thermal degradation, and somewhat unstable; consequently, attempts have been made to improve its properties by adding other synergistic materials.[26] For example, Zhang et al.[27] constructed a nanocomposite 3D interconnected architecture by sandwiching PPy nanowires between graphene nanolayers, which enhanced the thermoelectric performance. Conductive polymer/CNT composites may be synthesized by in situ chemical oxidative polymerization, electrochemical polymerization, or noncovalent functionalization.[28−30] Although electrochemical polymerization yields composites that are more conductive than those produced by chemical oxidative polymerization, it is unsuitable for large-scale production.

Polyurethanes (PUs) are generally synthesized by reacting isocyanate (−NCO) with polyols, which form the hard and soft segments, respectively.[31] The resulting segmented structure endows PUs with both high strength and excellent elasticity. PUs are widely used in mechanical, medical, and electronic applications. Many researchers have developed EMI shielding materials by adding a hybrid filler to PU to create polymer nanocomposites. For instance, Ramôa et al.[32] reported an EMI SE of 22 dB at 8−12 GHz for a PU/CNT composite with 10 wt % CNTs. Jia et al.[33] prepared a PU/graphite fiber/MXene-wrapped ammonium polyphosphate composite with a maximum EMI SE of 58.6 dB at 8.2−12.4 GHz. Avadhanam et al.[34] reported an EMI SE of 11 dB at 8−12 GHz for a single-walled CNT−polyaniline core−shell/PU polymer composite with 3 wt % CNTs. Verma et al.[35] prepared a GNP/CNT/PU composite with a maximum EMI SE of 47 dB at 8.2−12.4 GHz.

In this work, we report the successful synthesis of a 3D GNP/multiwalled CNT (MWCNT)/PPy hybrid filler by in situ chemical oxidative polymerization. The unique porosity of MWCNTs creates networks that enable electrolyte dispersion through the material; when combined with PPy, it further enhances the electrical conductivity and charge transfer behavior of the composite.[36] GNPs, which have high conductivity and an excellent EMI SE,[37] were also added to the composite. It was coated with PPy, which improved its dispersion. In the hybrid filler, the MWCNTs served as conductive bridges, which also increased the basal spacing between GNP sheets.[38] The GNP/MWCNT/PPy hybrid filler was analyzed by field emission scanning electron microscopy (FE-SEM), Raman spectroscopy, fast Fourier transform infrared (FTIR) spectroscopy, UV−visible light (UV−vis) spectroscopy, and resistivity tests. Finally, the GNP/MWCNT/PPy hybrid filler was incorporated into a PU matrix to form a nanohybrid with conductive 3D networks. A comparative analysis was performed by conducting EMI shielding tests on the nanohybrid, MWCNT/PPy/PU, and GNP/PPy/PU.

2. EXPERIMENTAL SECTION

2.1. Materials. Pyrrole (Py) monomers (C_4H_4NH) were purchased from Tokyo Chemical Industries Co., Ltd. Ferric chloride hexahydrate ($FeCl_3·6H_2O$) and hydrochloric acid (HCl) were purchased from Wako Pure Chemical Industries, Ltd. Hexadecyltrimethylammonium bromide (CTAB) ($C_{19}H_{42}BrN$) was purchased from Acros Organics. Methanol (CH_3OH) was purchased from Zimi Chemicals Co., Ltd. Dimethylformamide (DMF) was purchased from Sigma-Aldrich Co., Ltd. Methyl ethyl ketone (MEK) was purchased from Echo Chemicals Co., Ltd. PU with a molecular weight of 70,000 was purchased from Chia Yong Co., Ltd. The industrial grade MWCNTs used in this study had diameters of 10−25 nm, a length of 10 μm, a purity of at least 95%, and a Brunauer−Emmett−Teller (BET) specific surface area of 110−250 m^2/g. The GNPs used in this study had an oxygen content of ≤3 wt %, average thickness (Z axis) of 5 nm, average lateral sizes (X−Y plane) of D_{50} = 11 ± 3 μm and D_{95} ≤ 25 μm, and a BET specific surface area of 20−30 m^2/g.

2.2. Synthesis of Conducting Hybrid Fillers. Pure PPy and the MWCNT/PPy and GNP/PPy hybrid fillers were synthesized by in situ chemical oxidative polymerization. Solutions (300 mL) of 0.1 M HCl and 0.03 M CTAB were prepared in reaction flasks, which were magnetically stirred at room temperature. MWCNTs and GNPs (0, 2, 4, and 8 g) were added to these solutions, which were then ultrasonicated. The Py monomer was then added dropwise to these solutions with magnetic stirring, up to a concentration of 0.086 M. As a $FeCl_3$/Py ratio of approximately 2.3 is considered optimal,[39] $FeCl_3·6H_2O$ was added dropwise up to a concentration of 0.2 M. Polymerization was then performed at 0−5 °C with stirring for 4 h. The obtained MWCNT/PPy and GNP/PPy precipitates were filtered out of the solution using a water aspirator pump. The precipitates were washed several times with distilled water and methanol, heated to 80 °C for 6 h, and ground into a powder, which was then dried in a vacuum furnace. To prepare the GNP/MWCNT/PPy hybrid filler, MWCNTs and GNPs were mixed at weight ratios of 25/75, 33/67, 50/50, 67/33, and 75/25. Each mixture was added to a separate aqueous solution of 0.03 M CTAB and 0.1 M HCl. These solutions were then ultrasonicated. In situ chemical oxidative polymerization was performed by adding Py up to a concentration of 0.086 M with stirring, followed by the dropwise addition of $FeCl_3·6H_2O$ up to 0.2 M. The solution was stirred for 4 h at 0−5 °C to obtain GNP/MWCNT/PPy precipitates. These precipitates were filtered out using a water aspirator pump and repeatedly washed with distilled water and methanol. They were heated at 80 °C for 6 h, ground to a powder, and dried in a vacuum furnace. In addition, GNP/MWCNT/PPy materials with higher PPy contents were also prepared to obtain a GNP/MWCNT/PPy hybrid filler with 3D structure.

2.3. Preparation of GNP/MWCNT/PPy/PU Nanocomposites. A solvent consisting of DMF and MEK was prepared. Butanone was added to lower its boiling point so that the solvent could be fully volatilized at a temperature below the melting point of PU. PU was dissolved in this solvent at room temperature with stirring for 1 h. MWCNT/PPy, GNP/PPy, and GNP/MWCNT/PPy hybrid fillers were added at various ratios to the PU solution with stirring for 10 min at 300 rpm to produce a homogeneous slurry. These slurries were then used to prepare 1.5 mm thick nanohybrid sheets, which were dried in an oven. Various GNP/MWCNT/PPy/PU nanocomposites were obtained in this way.

2.4. Characterization and Instruments. EMI SE measurements were performed according to the ASTM

https://doi.org/10.1021/acsomega.2c06613
ACS Omega 2022, 7, 45697−45707

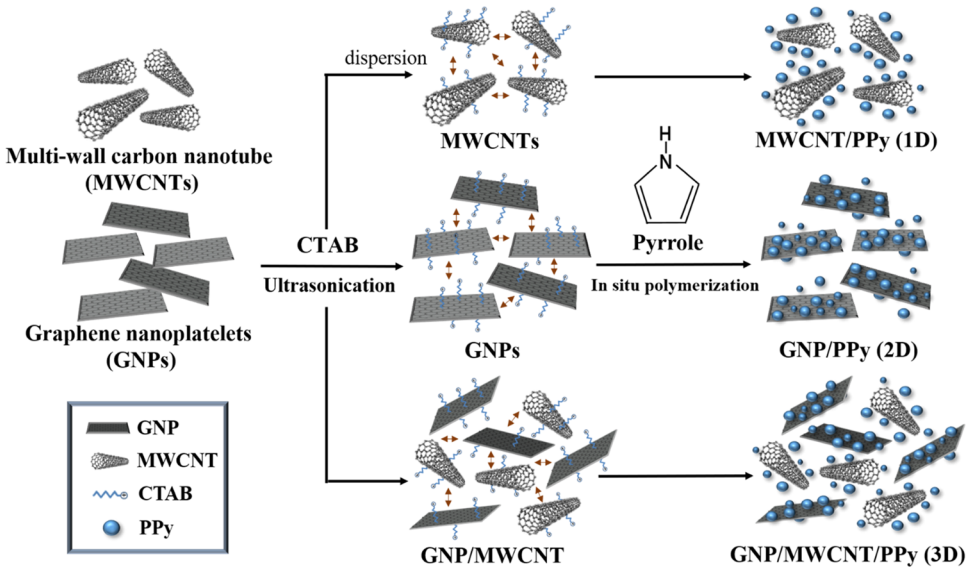

Figure 1. Illustration of the proposed adsorption mechanism, which explains the stable dispersion of GNP/MWCNT/PPy nanohybrids according to their molecular interactions, and the formation of hybrid fillers with various dimensionalities by in situ chemical oxidative polymerization..

Table 1. Sample Parameters of Synthesized Hybrid Fillers and Nanohybrids Formed by Their Incorporation into a PU Matrix

	hybrid fillers					
sample	GNPs (g)	MWCNTs (g)	PPy (g)	electrical conductivity (S/cm)[a]	PU (g)	EMI SE (dB)[b]
MWCNT/PPy (1:2)	0	2	4.0	1.2	35	1−7
MWCNT/PPy (2:2)	0	4	3.8	1.5	35	8−13
MWCNT/PPy (4:2)	0	8	4.1	1.8	35	15−20
GNP/PPy (1:2)	2	0	4.2	2.1	35	1−5
GNP/PPy (2:2)	4	0	4.4	2.5	35	5−10
GNP/PPy (4:2)	8	0	3.9	2.7	35	10−15
(GNP/MWCNT)(50/50)/PPy (2:2)	2	2	3.8	17.5	35	4−9
(GNP/MWCNT)(67/33)/PPy (3:2)	4	2	4.2	23.2	35	10−15
(GNP/MWCNT)(75/25)/PPy (4:2)	6	2	4.3	27.7	35	18−23
(GNP/MWCNT)(33/67)/PPy (3:2)	2	4	4.2	18.8	35	18−22
(GNP/MWCNT)(25/75)/PPy (4:2)	2	6	3.9	21.7	35	25−30
(GNP/MWCNT)(25/75)/PPy (4:3)	2	6	6.2	4	35	27−32
(GNP/MWCNT)(25/75)/PPy (4:4)	2	6	8.3	7.7	35	35−40

[a]Electrical conductivity was measured by molding hybrid fillers into 10 mm × 0.5 mm disks using a compression molder operating at 300 kgf/cm^2 and then performing conductivity measurements using a four-point probe. [b]A VNA was used according to the ASTM D4935-99 method to determine the scattering parameters of the nanohybrids, which were then used to calculate the EMI SE. The measured frequency range was 30−1800 MHz.

D4935-99 standard using a vector network analyzer (VNA; Hewlett-Packard 8510c) and a flanged circular coaxial transmission line holder. The frequency range was 30−1800 MHz. A four-point probe resistivity meter (Mitsubishi Chemical Corporation, MCP-T600) was used to measure the electrical conductivity of the hybrid fillers. Before these measurements, a compression molder was used to compress the hybrid filler samples at a pressure of 300 kgf/cm^2 into disks with a diameter of 10 mm and thickness of 0.5 mm. FE-SEM was performed (JEOL, JSM-6500F) at 10 kV to observe the surface morphology of the hybrid fillers and nanohybrids. Before FE-SEM analysis, each sample was fixed using a conductive carbon paste and coated with a Pt film. The surface morphologies of the hybrid fillers were also analyzed by transmission electron microscopy (TEM) (FEI, Tecna G2 F-20 S-TWIN) at 200 kV. For these measurements, the samples were first diluted in pure water and dropped onto a carbon-coated copper mesh, which was then dried for 12 h at 80 °C in an oven. Raman spectroscopy was performed at 600−2000 cm^{-1} using a Horiba iHR550 Raman spectrometer with an Olympus BX-41 microscope and a 5 mW, 532 nm laser source. FTIR spectroscopy was performed at 600−2000 cm^{-1} using a Jasco FT/IR-300E instrument; each FTIR spectrum was obtained by averaging 16 scans. UV−vis spectroscopy (Shimadzu UV-2450) was performed to analyze the transmission characteristics of PPy, MWCNT/PPy, GNP/PPy, and GNP/MWCNT/PPy at 250−800 nm. The hybrid filler samples were dissolved in DMF for these measurements.

3. RESULTS AND DISCUSSION

3.1. Dispersion and Microstructure of GNP/MWCNT/PPy Hybrid Fillers. We prepared various hybrid fillers with different dimensionalities for two reasons. The first goal was to optimize the synergistic effect between CNTs and PPy and thus improve the electrical conductivity. To this end, a cationic surfactant (CTAB) was added to various CNTs and sonicated,

https://doi.org/10.1021/acsomega.2c06613
ACS Omega 2022, 7, 45697−45707

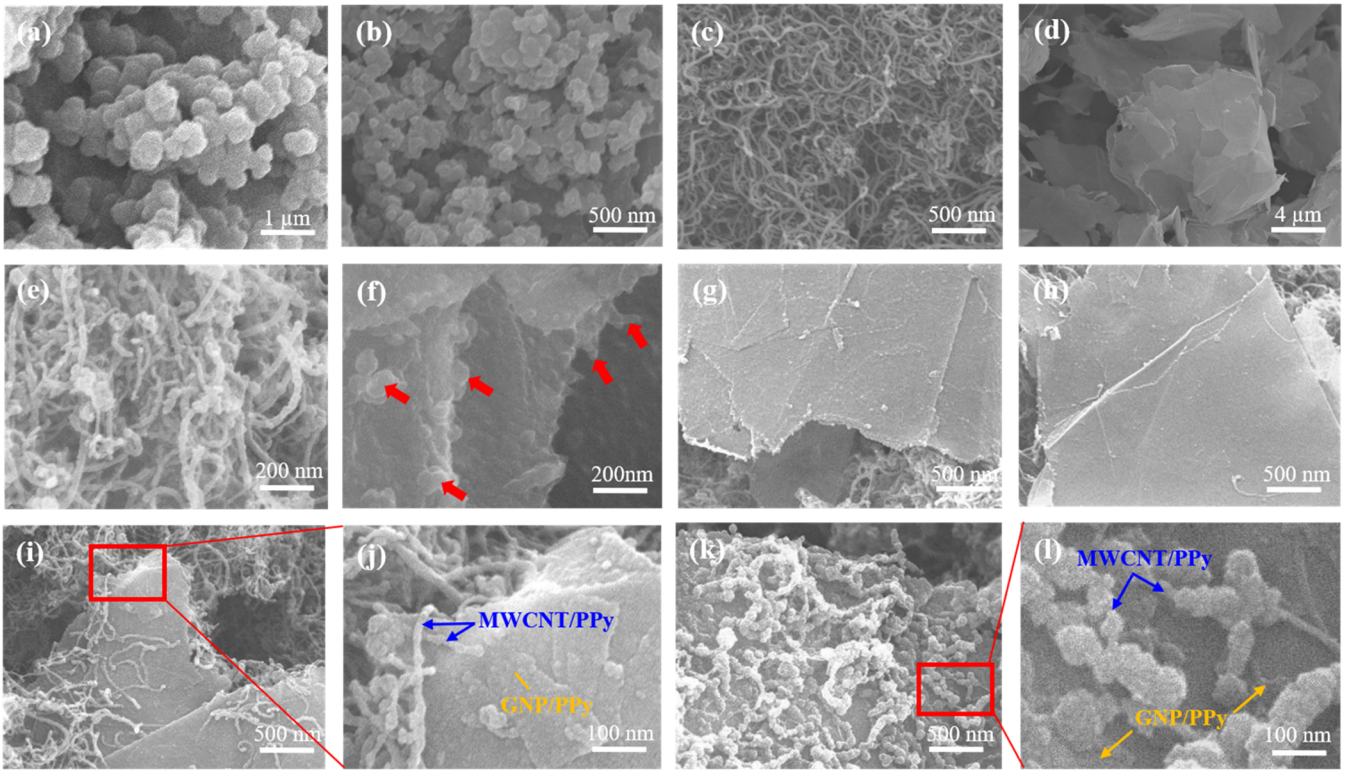

Figure 2. FE-SEM images of hybrid fillers: (a) PPy, (b) PPy with 0.03 M CTAB, (c) MWCNTs, (d) GNPs, (e) MWCNT/PPy (4:2), (f) GNP/PPy (4:2), (g) (GNP/MWCNT) (75/25)/PPy (4:2), (h) (GNP/MWCNT) (25/75)/PPy (4:2), (i, j) (GNP/MWCNT) (25/75)/PPy (4:3) at different magnifications, and (k, l) (GNP/MWCNT) (25/75)/PPy (4:4) at different magnifications.

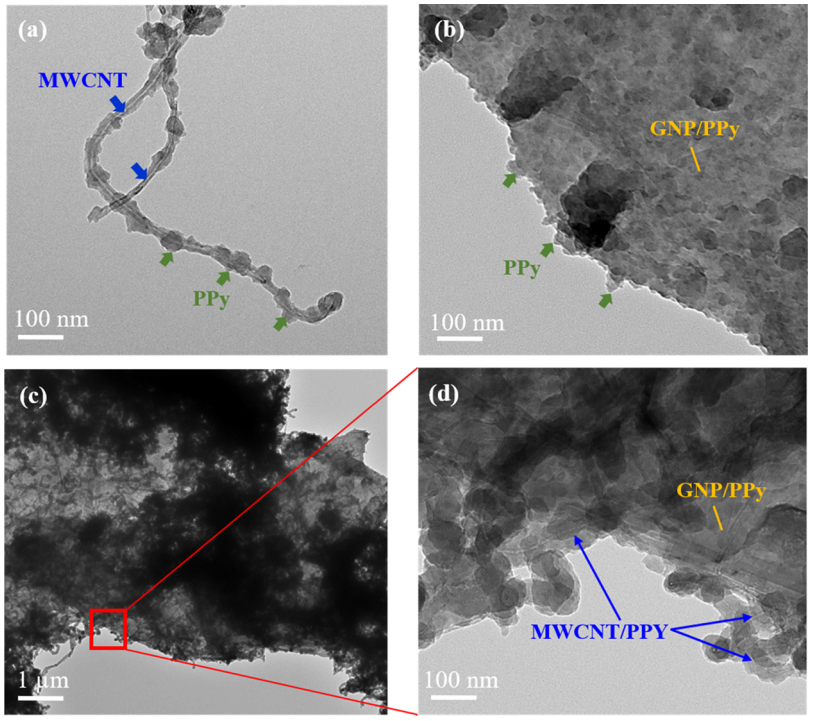

Figure 3. TEM images of hybrid fillers: (a) MWCNT/PPy (4:2), (b) GNP/PPy (4:2), and (c, d) (GNP/MWCNT) (25/75)/PPy (4:4) at different magnifications.

and in situ chemical oxidative polymerization was performed to prepare PPy/CNT hybrid fillers. The second goal was to fabricate multidimensional hybrid fillers, that is, MWCNT/PPy (1D), GNP/PPy (2D), and GNP/MWCNT/PPy (3D), by combining MWCNTs (1D) with GNPs (2D) and PPy (0D). The nanodispersion process is illustrated in Figure 1. Table 1 shows the formulations of the PU nanocomposites that

https://doi.org/10.1021/acsomega.2c06613
ACS Omega 2022, 7, 45697−45707

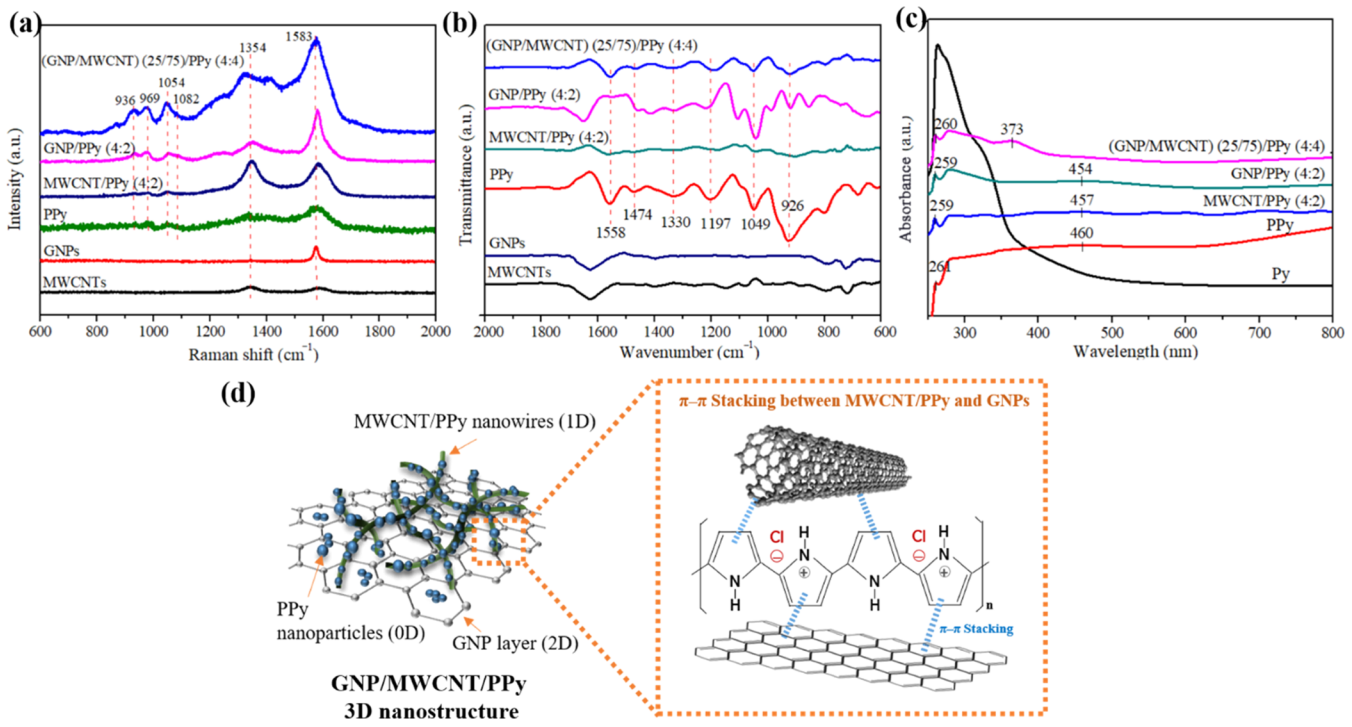

Figure 4. Spectroscopic data of hybrid fillers: (a) Raman spectra, (b) FTIR spectra, and (c) UV−vis spectra. (d) Illustration of 3D nanostructure of GNP/MWCNT/PPy and interactions between GNPs, MWCNTs, and PPy.

were formed by incorporating MWCNT/PPy, GNP/PPy, and GNP/MWCNT/PPy hybrid fillers into a PU matrix.

Figure 2a shows an FE-SEM micrograph of PPy synthesized by in situ chemical oxidative polymerization without CTAB. It appears as tightly aggregated irregular spheres with an average grain size of 300 nm. This result is consistent with the appearance of PPy reported in previous studies.[40] After CTAB addition, the Py monomers become encapsulated in micelles, which reduces the average grain size of the synthesized PPy,[41] as shown in Figure 2b. Figure 2c shows the string-like structure of the MWCNTs, whereas Figure 2d shows that the GNPs have a smooth, curved sheet-like structure. MWCNT/PPy, GNP/PPy, and GNP/MWCNT/PPy hybrid fillers were prepared by adding CTAB. Previous studies have demonstrated that CTAB improves the dispersion of MWCNTs and GNPs and also the electrical conductivity of PPy.[42,43] In the MWCNT/PPy (4:2) hybrid filler (Figure 2e), the smooth MWCNT surfaces are covered by spherical PPy particles. Therefore, the interaction between PPy and the MWCNTs is strong enough to overcome inter-MWCNT van der Waals interactions.[44] In the GNP/PPy (4:2) hybrid filler (Figure 2f), the surfaces of the GNP sheets are unevenly covered by PPy particles, and the protrusions on the edges of the GNP sheets (red arrows) are deposits formed by PPy particles. Furthermore, the attachment of PPy particles weakens the van der Waals interactions between the GNP sheets, thus reducing GNP aggregation.[45]Figure 2g,h shows the surface morphologies of the (GNP/MWCNT) (75/25)/PPy (4:2) and (GNP/MWCNT) (25/75)/PPy (4:2) hybrid fillers, respectively. Here, the GNP surfaces are covered by a thin layer of PPy. However, no MWCNT attachment was observed in either sample. When the proportion of PPy was increased (Figure 2i,j), microstructures containing interconnected MWCNT/PPy nanowires (1D) and GNP/PPy nanolayers (2D) began to appear. The surface morphology of the (GNP/MWCNT) (25/75)/PPy (4:4) hybrid filler, which contains the highest proportion of PPy, is shown in Figure 2k,l. Two-dimensional GNP/PPy nanolayers are extensively covered by 1D MWCNT/PPy nanowires, which are interconnected to form a 3D network. The MWCNT/PPy nanowires have diameters of 30−100 nm, and they are clearly attached to the GNP/PPy nanolayers (that is, they are not suspended at a distance from the GNP/PPy surface). As mentioned above, the deposition of additional PPy weakens the van der Waals interactions of the MWCNTs and GNPs, increasing their dispersion. Furthermore, the PPy, MWCNTs, and GNPs may interact with each other via hydrogen bonds or $\pi-\pi$ stacking,[27] resulting in the formation of a GNP/MWCNT/PPy 3D network nanostructure.

Figure 3a shows a TEM micrograph of the MWCNT/PPy (4:2) hybrid filler, which clearly shows the hollow structure and crystalline sidewalls of the MWCNTs and the PPy enveloping the MWCNTs in a classic core−shell structure. The PPy layer on the MWCNT surface is <30 nm thick. Figure 3b shows the GNP/PPy (4:2) hybrid filler, where a layer of PPy was clearly deposited on the GNP sheets. PPy nanorods also appear around the edges of the GNP sheets. In Figure 3c,d, the GNP sheets are extensively covered by tightly adhering PPy particles and MWCNT/PPy nanowires, where the nanowires are up to a few microns long. Because of the higher PPy content, the thickness of the PPy shell on the MWCNTs increased to <80 nm. Therefore, it may be concluded that the (GNP/MWCNT) (25/75)/PPy (4:4) hybrid filler is an interconnected 3D structure formed by the stacking of MWCNT/PPy nanowires (1D) on GNP/PPy nanolayers (2D).

3.2. Structural Characterization of the GNP/MWCNT/PPy Hybrid Filler and Its Intercomponent Interactions.

Raman, FTIR, and UV−vis spectroscopy were used to characterize the structure of the MWCNT/PPy, GNP/PPy,

https://doi.org/10.1021/acsomega.2c06613
ACS Omega 2022, 7, 45697−45707

and GNP/MWCNT/PPy hybrid fillers and the interactions between the MWCNTs, GNPs, and PPy. Figure 4a shows the Raman spectra of the MWCNTs, GNPs, PPy, and MWCNT/PPy (4:2), GNP/PPy (4:2), and (GNP/MWCNT) (25/75)/PPy (4:4) hybrid fillers. The MWCNT spectrum has two strong peaks at 1332 and 1588 cm^{-1}. The former is the disorder (D) band, which represents crystal defects in the CNTs, that is, sp^3 bonds. The latter is the graphite (G) band, which indicates the crystallinity of the graphite layer, that is, sp^2 bonds.[46] The GNP spectrum has two peaks, one near the D band at 1339 cm^{-1} and a relatively strong peak near the G band at 1576 cm^{-1}.[47] The main characteristic peak of the PPy spectrum is the 931 cm^{-1} peak, which represents C−H ring deformation in the bipolaron structure. The peaks at 971, 1053, 1082, and 1238 cm^{-1} represent C−H ring deformation in the polaron structure, C−H in-plane bending in the polaron structure, symmetric C−H in-plane bending in the bipolaron structure, and N−H in-plane deformation, respectively. The characteristic peaks at 1376 and 1583 cm^{-1} are attributed to C−N and C═C stretching, respectively. In the MWCNT/PPy, GNP/PPy, and GNP/MWCNT/PPy spectra, the peaks at 969 and 1054 cm^{-1} indicate a quinonoid polaronic structure, whereas the 936 and 1082 cm^{-1} peaks indicate a quinonoid bipolaronic structure. Therefore, these structures possess some bipolarity and also contain PPy (Cl^-). In contrast to those in the MWCNTs and GNPs spectra, the 1576 cm^{-1} peak is blue-shifted to 1583 cm^{-1} in the MWCNT/PPy, GNP/PPy, and GNP/MWCNT/PPy spectra. We speculate that this blue shift is caused by $\pi-\pi$ stacking between the C═C bonds of PPy and those of the MWCNTs and GNPs.[47,48] Furthermore, the D and G bands are both broader and more intense in the MWCNT/PPy, GNP/PPy, and GNP/MWCNT/PPy spectra. Because the intensity of the G band is proportional to the planar crystallite size of graphite, this result indicates increased polymer thickness due to the envelopment of GNPs by PPy.[45]

Figure 4b shows the FTIR spectra of the MWCNTs, GNPs, PPy, and MWCNT/PPy (4:2), GNP/PPy (4:2), and (GNP/MWCNT) (25/75)/PPy (4:4) hybrid fillers. The signal at 1623 cm^{-1} in the MWCNTs and GNPs spectra is attributed to the O−H bending mode of water and C═C stretching vibrations in the MWCNTs and GNPs. The peak at 1453 cm^{-1} is due to CH or CH_2 bending vibrations, whereas the small peak at 1050 cm^{-1} is attributed to cyclic C−O−C bonds. The main characteristic peaks of pure PPy are located at 1558 and 1474 cm^{-1} and indicate antisymmetric and symmetric ring-stretching modes, respectively. The other notable absorption peaks in the PPy spectrum are located at 1330 cm^{-1} (C−H and C−N in-plane deformation), 1049 cm^{-1} (C−H and N−H in-plane deformation), 1197 cm^{-1} (Py ring breathing), and 926 cm^{-1} (C−H out-of-plane deformation).[48−50] The main IR absorption modes of the MWCNT/PPy, GNP/PPy, and GNP/MWCNT/PPy hybrid fillers have analogous bands in the FTIR spectra of pure GNPs, MWCNTs, and PPy. Comparisons with the pure PPy spectrum reveal that the intensity of the C−H band changed dramatically when MWCNTs and GNPs were added during the synthesis of PPy. Therefore, the PPy backbone could be interacting with MWCNTs and GNPs via $\pi-\pi$ stacking.

Figure 4c shows the UV−vis spectra of Py, pure PPy, MWCNT/PPy (4:2), GNP/PPy (4:2), and (GNP/MWCNT) (25/75)/PPy (4:4). The main absorption peak of Py is located at 290 nm.[51] PPy, which is obtained by the chemical polymerization of Py monomers, has a main absorption peak at 261 nm. The location of this peak could be attributed to the $\pi-\pi^*$ transition of the aromatic ring. The PPy spectrum also has a broad peak around 400−500 nm, with a maximum at 460 nm. This peak represents the polaron state of PPy, and it demonstrates that PPy was successfully polymerized from Py monomers. In the spectra of the MWCNT/PPy (4:2) and GNP/PPy (4:2) hybrid fillers, the PPy peaks are blue-shifted (from 261 to 259 nm, and from 460 to 457 and 454 nm, respectively). This change indicates that the band gap between the π and π^* orbitals expanded because of the strengthening of conjugated π bonds, which could be caused by strong interactions between PPy and the MWCNTs and GNPs. In addition to the peak at 260 nm, the (GNP/MWCNT) (25/75)/PPy (4:4) hybrid filler also has a significant peak at 373 nm, which corresponds to a transition from the valence band to the antibonding polaron state in PPy. This peak can be attributed to the higher PPy content of this hybrid filler.[48,52,53]

The Raman, FTIR, and UV−vis data indicate that in situ chemical oxidative polymerization formed PPy doped with Cl^- [PPy(Cl^-)], which successfully adhered to the surfaces of MWCNTs and GNPs. Therefore, MWCNT/PPy, GNP/PPy, and GNP/MWCNT/PPy hybrid fillers were successfully synthesized, and PPy may interact with MWNCTs and GNPs via $\pi-\pi$ stacking. According to Figures 2k,l and 3c,d, the 3D nanostructure of the GNP/MWCNT/PPy hybrid filler consists of GNP layers (2D) that are extensively covered by PPy (0D) and MWCNT/PPy nanowires (1D), which interact via $\pi-\pi$ stacking. An illustration of these interactions is shown in Figure 4d.

3.3. Electrical Conductivity of the GNP/MWCNT/PPy Hybrid Filler. The EMI SE of a nanohybrid can be improved by increasing the electrical conductivity of its filler.[54] The electrical conductivities of the MWNCT/PPy, GNP/PPy, and GNP/MWCNT/PPy hybrid fillers were measured using 10 mm × 0.5 mm disk samples of each filler obtained using a compression molder (as shown in Figure 5a−c). A four-point probe was used for the measurement; the results are shown in Figure 5. The PPy prepared with added CTAB has an electrical

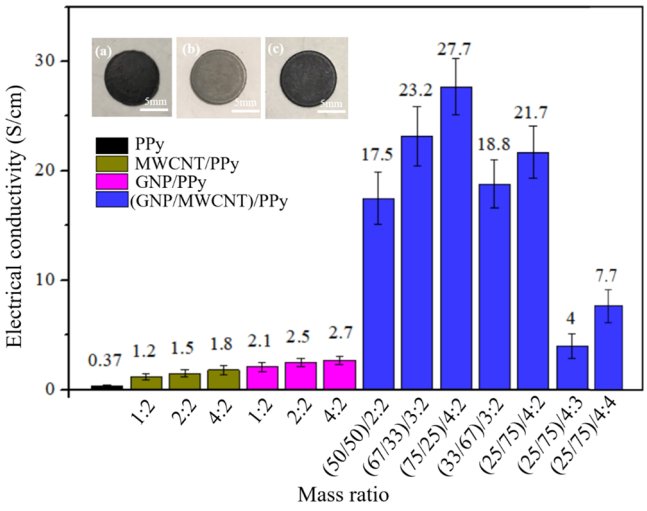

Figure 5. Electrical conductivities of PPy, MWCNT/PPy, GNP/PPy, and GNP/MWCNT/PPy hybrid fillers with different formulations. Insets show digital photographs of disk samples of (a) MWCNT/PPy (4:2), (b) GNP/PPy (4:2), and (c) (GNP/MWCNT) (25/75)/PPy (4:4).

https://doi.org/10.1021/acsomega.2c06613
ACS Omega 2022, 7, 45697−45707

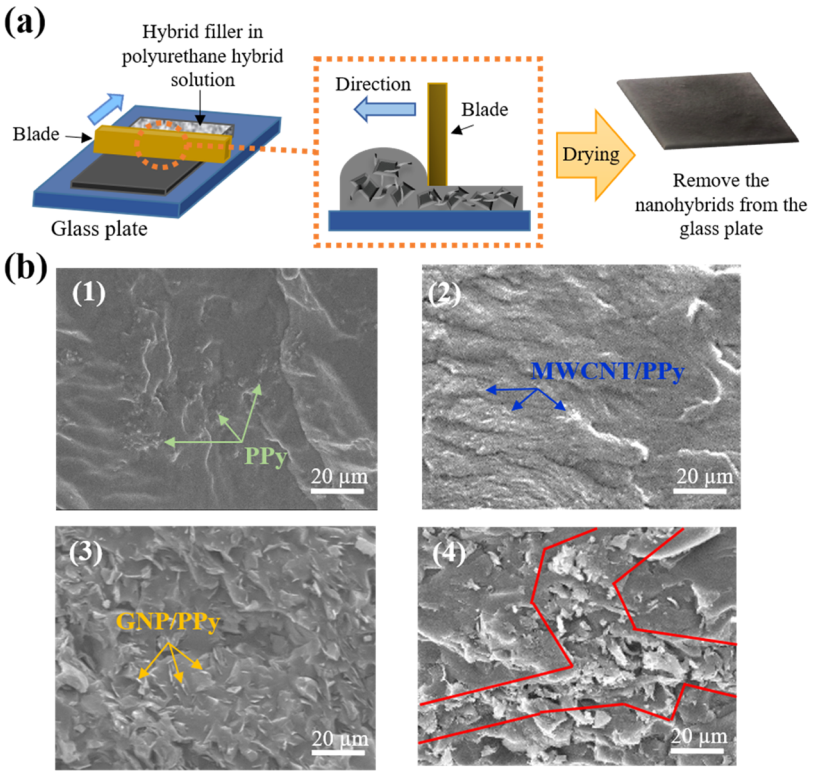

Figure 6. (a) Preparation of nanohybrids from hybrid filler−PU mixture using blade coating method. (b) FE-SEM micrographs of each hybrid filler in PU matrix: (1) PPy/PU, (2) MWCNT/PPy (4:2)/PU, (3) GNP/PPy (4:2)/PU, and (4) (GNP/MWCNT) (25/75)/PPy (4:4)/PU.

conductivity of 0.37 S/cm. The electrical conductivities of MWCNT/PPy and GNP/PPy were significantly higher because of the high aspect ratios and specific surface areas of GNPs and MWCNTs. This result can also be attributed to $\pi-\pi$ stacking between PPy and the MWNCTs and GNPs, which provides a path for electrical conduction between these molecules. Furthermore, the long conjugation lengths resulting from the very slow polymerization rate facilitate electron conduction along the PPy backbone.[50,55] In the MWCNT/PPy and GNP/PPy hybrid fillers, higher MWCNT and GNP contents generally resulted in higher conductivity. For instance, the MWCNT/PPy (4:2) and GNP/PPy (4:2) hybrid fillers have conductivities of 1.8 and 2.7 S/cm, respectively. The electrical conductivities of the GNP/MWCNT/PPy hybrid fillers (with a fixed PPy content) are 17.5 S/cm for (GNP/MWCNT) (50/50)/PPy (2:2), 27.7 S/cm for (GNP/MWCNT) (75/25)/PPy (4:2), and 21.7 S/cm for (GNP/MWCNT) (25/75)/PPy (4:2). These values are much higher than those of the MWCNT/PPy and GNP/PPy hybrid fillers owing to $\pi-\pi$ interactions between PPy and the MWCNTs and GNPs. However, when the PPy content was increased further, the thickness of PPy coating on GNP and MWCNT increased significantly. Therefore, the electrical conductivity fell to 4.1 S/cm in the (GNP/MWCNT) (75/25)/PPy (4:3) hybrid filler and then increased slightly to 7.7 S/cm in the (GNP/MWCNT) (75/25)/PPy (4:4) hybrid filler. We speculate that the reason could be the tendency of dispersion to increase as MWCNT/PPy nanowires are deposited on the GNP/PPy nanolayers, which improves the electrical conductivity of the interconnected conductive network.

3.4. Surface Morphology and EMI SE of Nanohybrids Formed by the Incorporation of GNP/MWCNT/PPy Hybrid Filler into the PU matrix. The process by which hybrid fillers are incorporated into PU to form a nanohybrid is shown in Figure 6a. We used the blade coating method, a facile method of nanocomposite preparation.[56] The solution containing the hybrid filler−PU mixture is first coated onto a glass plate and then dried (with heating) to evaporate the solvent. Finally, the material is peeled from the glass plate to obtain a flat, uniform film. PPy/PU, GNP/PPy/PU, MWCNT/PPy/PU, and (GNP/MWCNT)/PPy/PU nanohybrids were obtained in this way. FE-SEM was used to observe the dispersion of each hybrid filler in the PU matrix. In Figure 6b(1), the circular protrusions are pure PPy in the PU matrix. MWCNT/PPy appears as aggregated small circular white spots in the PU matrix [Figure 6b(2)], whereas GNP/PPy appears as short white lines evenly dispersed in the PU matrix [Figure 6b(3)]. In the FE-SEM micrograph of the (GNP/MWCNT) (25/75)/PPy (4:4)/PU composite [Figure 6b(4)], the hybrid filler exhibits molecular stacking, which could be caused by its 3D nanostructure and synergistic effects between its components. Furthermore, a continuous and electrically conductive network clearly formed in the PU matrix.

Electromagnetic shielding is defined as the ability of a material to shield an electronic device from the effects of electromagnetic radiation. The EMI SE quantifies the attenuation of electromagnetic radiation in decibels, and it is given by

$$\text{EMI SE} = 10\log(P_i/P_t) = 20\log(E_i/E_t)$$

In this equation, P_i (E_i) and P_t (E_t) are the power (electric field intensity) of the incident and transmitted electromagnetic waves, respectively. Higher SE values (dB) indicate greater attenuation of electromagnetic radiation. Furthermore, a 10 dB increase in EMI SE indicates that scattering has increased by

https://doi.org/10.1021/acsomega.2c06613
ACS Omega 2022, 7, 45697−45707

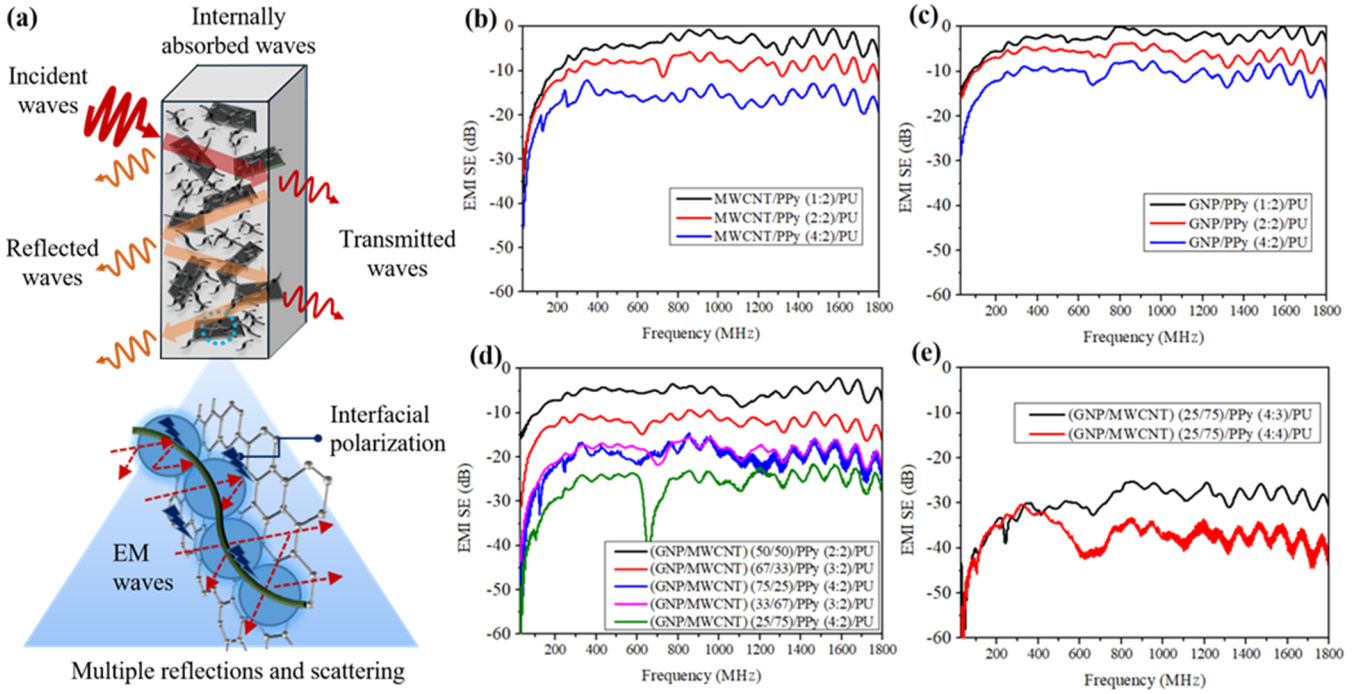

Figure 7. (a) EMI SE mechanism of GNP/MWCNT/PPy/PU nanohybrid. EMI SEs of (b) MWCNT/PPy/PU with different MWCNT contents; (c) GNP/PPy/PU with different GNP contents; (d) (GNP/MWCNT)/PPy/PU with different MWCNT and GNP contents; and (e) (GNP/MWCNT)/PPy/PU with different PPy contents.

an order of magnitude. For instance, SEs of 30 and 40 dB indicate that 99.9% and 99.99% of the incident electromagnetic waves are blocked, respectively. Shielding materials with an SE of 30 dB are generally considered adequate for recent commercial applications. The mechanism of the EMI SE may be explained using transmission line theory,[57] as shown in Figure 7a. When an electromagnetic wave reaches the surface of the shielding material, the wave is partially reflected, and the rest of the wave propagates into the material. The propagating electromagnetic waves are weakened by absorption by the material, and they also undergo losses due to re-reflection and multiple reflections between the front and rear interfaces of the material. According to Schelkunoff theory, the EMI SE of a material may be expressed as

$$SE(dB) = SE_A + SE_R + SE_M$$

In this equation, SE_A is the absorption loss in the material, and SE_R and SE_M are the reflection and multiple reflection losses, respectively.[58,59] In this study, the EMI SEs of the MWCNT/PPy/PU, GNP/PPy/PU, and GNP/MWCNT/PPy/PU nanohybrids were derived from scattering parameters measured using a VNA.

The EMI SE of the MWCNT/PPy/PU, GNP/PPy/PU, and GNP/MWCNT/PPy/PU nanohybrids was measured at 30−1800 MHz. The effect of MWCNT content on the EMI SE of MWCNT/PPy hybrid fillers with a fixed proportion of PPy is shown in Figure 7b. As expected, the EMI SE is positively correlated with the MWCNT content. The optimal EMI SE (15−20 dB) was found in the filler with 8 g of MWCNTs (the highest MWCNT content). The improvement in EMI SE due to higher MWCNT content may be attributed to the formation of conductive networks in the PU matrix by the MWCNT/PPy hybrid filler. As MWCNTs have high specific surface areas and aspect ratios, they can combine with the conductive region of PPy to form conductive bridges and thus increase the effective permeability, which facilitates the formation of an extensive conductive network. The effects of GNP content on the EMI SE of GNP/PPy hybrid fillers with a fixed proportion of PPy are shown in Figure 7c. These results qualitatively resemble those of the MWCNT/PPy hybrid filler, as the EMI SE also improved with increasing GNP content. The GNP/PPy hybrid filler with 8 g of GNPs has EMI SEs of 10−15 dB. As the number of electrically conductive networks in the PU matrix depends on the GNP content, the EMI SE will naturally improve with increasing GNP content. A comparison of the EMI SEs of MWCNT/PPy and GNP/PPy reveals that MWCNTs outperform GNPs for the same weight of carbon. The EMI SEs of GNP/MWCNT/PPy hybrid fillers with different GNP and MWCNT contents and a fixed proportion of PPy are shown in Figure 7d. The EMI SE is positively correlated with the carbon content. However, MWCNTs clearly have a more significant effect on the EMI SE, as the EMI SEs of (GNP/MWCNT) (75/25)/PPy (4:2)/PU and (GNP/MWCNT) (25/75)/PPy (4:2)/PU are approximately 18−23 and 25−30 dB, respectively. The electrical conductivities obtained by a four-point probe resistivity meter are 0.02 S/cm for (GNP/MWCNT) (75/25)/PPy (4:2)/PU, and 0.07 S/cm for (GNP/MWCNT) (25/75)/PPy (4:2)/PU. Although (GNP/MWCNT) (25/75)/PPy (4:2)/PU, MWCNT/PPy (4:2)/PU, and GNP/PPy (4:2)/PU have the same carbon and PPy contents by weight, mixing GNPs with MWCNTs significantly improves the EMI SE. We hypothesize that the reason is synergies between GNPs, MWCNTs, and PPy, which allow MWCNTs to form wide conjugated networks and fill gaps between GNP sheets. PPy also suppresses the aggregation of MWCNTs and GNPs. Interfacial polarization between GNPs, MWCNTs, PPy, and PU may also enhance the EMI SE.[59,60] Figure 7e shows the effects of increasing PPy content at fixed GNP and MWCNT contents. (GNP/MWCNT) (25/75)/PPy (4:4)/PU has the highest EMI SE, 35−40 dB. The

https://doi.org/10.1021/acsomega.2c06613
ACS Omega 2022, 7, 45697−45707

result of the electrical conductivity test is 0.21S/cm, as shown in Video S1. As the GNP/MWCNT/PPy 3D nanostructure consists of MWCNT/PPy nanowires stacked on GNP/PPy nanolayers, it has a very wide interfacial surface. Furthermore, it forms a continuous network of GNP−PPy−CNT−PPy−GNP paths in the PU matrix. Therefore, the resulting nanohybrid has losses due to polarization, transmission, multiple reflections, and scattering, which combine to increase the reflectance and attenuation of electromagnetic waves.[61−63]

4. CONCLUSIONS

A facile and scalable method was used to prepare GNP/MWCNT/PPy hybrid fillers. MWCNTs form an extensive conjugated network that fills the gaps between GNP nanolayers and forms conductive bridges. PPy prevents the aggregation of MWCNTs and GNPs while allowing electron transmission through the PPy backbone. This synergy explains why GNP/MWCNT/PPy exhibits much higher electrical conductivity and EMI SE than GNP/PPy and MWCNT/PPy. When (GNP/MWCNT)/PPy was prepared with a mass ratio of (25/75)/4:4, the GNP/PPy nanolayers (2D) were extensively covered by MWCNT/PPy nanowires (1D), forming a hybrid filler with 3D nanostructure. The nanohybrid was formed by incorporating the hybrid filler into a PU matrix. Because of $\pi-\pi$ interactions between GNPs, MWCNTs, and PPy, a continuous network of GNP−PPy−CNT−PPy−GNP paths was formed within the PU insulator (as demonstrated by FE-SEM analysis). This network greatly enhances the reflectance and attenuation of electromagnetic waves. The optimal obtained nanohybrid has an EMI SE of 35−40 dB at 30−1800 MHz; therefore, it can shield over 99.9% of all electromagnetic waves within this frequency range. Therefore, this nanohybrid has great potential for commercial applications.

■ ASSOCIATED CONTENT

Supporting Information

The Supporting Information is available free of charge at https://pubs.acs.org/doi/10.1021/acsomega.2c06613.

Demonstration of conductive properties of (GNP/MWCNT)(25/75)/PPy(4:4)/PU nanohybrids. (Video S1) (MP4)

■ AUTHOR INFORMATION

Corresponding Author

Chih-Wei Chiu − *Department of Materials Science and Engineering, National Taiwan University of Science and Technology, Taipei 10607, Taiwan;* orcid.org/0000-0003-2258-2454; Phone: +886-2-2737-6521; Email: cwchiu@mail.ntust.edu.tw

Authors

Chih-Lung Lin − *Department of Materials Science and Engineering, National Taiwan University of Science and Technology, Taipei 10607, Taiwan*

Jia-Wun Li − *Department of Materials Science and Engineering, National Taiwan University of Science and Technology, Taipei 10607, Taiwan;* orcid.org/0000-0001-5033-2829

Yan-Feng Chen − *Department of Materials Science and Engineering, National Taiwan University of Science and Technology, Taipei 10607, Taiwan*

Jian-Xun Chen − *Department of Materials Science and Engineering, National Taiwan University of Science and Technology, Taipei 10607, Taiwan*

Chih-Chia Cheng − *Graduate Institute of Applied Science and Technology, National Taiwan University of Science and Technology, Taipei 10607, Taiwan;* orcid.org/0000-0002-1605-6338

Complete contact information is available at: https://pubs.acs.org/10.1021/acsomega.2c06613

Author Contributions

C.-L.L. performed data curation; C.-L.L., J.-W.L., Y.-F.C., J.-X.C., and C.-C.C. performed formal analysis; C.-W.C. performed supervision; C.-L.L. and C.-W.C. took care of writing—original draft; C.-L.L., J.-W.L., and C.-W.C. took care of writing—review and editing. All authors have read and agreed to the published version of the manuscript.

Notes

The authors declare no competing financial interest.

■ ACKNOWLEDGMENTS

This research was funded by the Ministry of Science and Technology (MOST 110-2622-E-011-028, MOST 111-2628-E-011-009-MY3, and MOST 111-2622-8-011-009-TE2) of Taiwan.

■ REFERENCES

(1) Sushmita, K.; Madras, G.; Bose, S. Polymer Nanocomposites Containing Semiconductors as Advanced Materials for EMI Shielding. *ACS Omega* **2020**, *5*, 4705−4718.

(2) Srivastava, S. K.; Manna, K. Recent Advancements in the Electromagnetic Interference Shielding Performance of Nanostructured Materials and Their Nanocomposites: A Review. *J. Mater. Chem. A* **2022**, *10*, 7431−7496.

(3) Sheng, A.; Ren, W.; Yang, Y.; Yan, D. X.; Duan, H.; Zhao, G.; Liu, Y.; Li, Z. M. Multilayer WPU Conductive Composites with Controllable Electro-Magnetic Gradient for Absorption-Dominated Electromagnetic Interference Shielding. *Composites, Part A* **2020**, *129*, No. 105692.

(4) Wanasinghe, D.; Aslani, F.; Ma, G.; Habibi, D. Review of Polymer Composites with Diverse Nanofillers for Electromagnetic Interference Shielding. *Nanomaterials* **2020**, *10*, No. 541.

(5) Chiu, C. W.; Huang, C. Y.; Li, J. W.; Li, C. L. Flexible Hybrid Electronics Nanofiber Electrodes with Excellent Stretchability and Highly Stable Electrical Conductivity for Smart Clothing. *ACS Appl. Mater. Interfaces* **2022**, *14*, 42441−42453.

(6) Huang, C. Y.; Chiu, C. W. Facile Fabrication of Stretchable and Flexible Nanofiber Carbon Film Sensing Electrode by Electrospinning and Its Application in Smart Clothing for ECG and EMG Monitoring. *ACS Appl. Electron. Mater.* **2021**, *3*, 676−686.

(7) Pawar, S. P.; Rzeczkowski, P.; Potschke, P.; Krause, B.; Bose, B. Does the Processing Method Resulting in Different States of an Interconnected Network of Multiwalled Carbon Nanotubes in Polymeric Blend Nanocomposites Affect EMI Shielding Properties? *ACS Omega* **2018**, *3*, 5771−5782.

(8) Li, J. W.; Huang, C. Y.; Zhou, B. H.; Hsu, M. F.; Chung, S. F.; Lee, W. C.; Tsai, W. Y.; Chiu, C. W. High Stretchability and Conductive Stability of Flexible Hybrid Electronic Materials for Smart Clothing. *Chem. Eng. J. Adv.* **2022**, *12*, No. 100380.

(9) Soong, Y. C.; Chiu, C. W. Multilayered Graphene/Boron Nitride/Thermoplastic Polyurethane Composite Films with High Thermal Conductivity, Stretchability, and Washability for Adjustable Cooling Smart Clothes. *J. Colloid Interface Sci.* **2021**, *599*, 611−619.

(10) Chiu, C. W.; Lin, C. A.; Hong, P. D. Melt-Spinning and Thermal Stability Behavior of TiO_2 Nanoparticle/Polypropylene Nanocomposite Fibers. *J. Polym. Res.* **2011**, *18*, 367−372.

(11) Ramoa, S. D. A. S.; Barra, G. M. O.; Merlini, C.; Livi, S.; Soares, B. G.; Pegoretti, A. Electromagnetic Interference Shielding Effectiveness and Microwave Absorption Properties of Thermoplastic Polyurethane/Montmorillonite-Polypyrrole Nanocomposites. *Polym. Adv. Technol.* **2018**, *29*, 1377−1384.
(12) Shukla, V. Role of Spin Disorder in Magnetic and EMI Shielding Properties of Fe_3O_4/C/PPy core/Shell Composites. *J. Mater. Sci.* **2020**, *55*, 2826−2835.
(13) Jin, B.; Meng, F.; Ma, H.; Zhang, B.; Gong, B.; Park, C. B.; Li, G. Synergistic Manipulation of Zero-Dimension and One-Dimension Hybrid Nanofillers in Multi-Layer Two-Dimension Thin Films to Construct Light Weight Electromagnetic Interference Material. *Polymers* **2021**, *13*, No. 3278.
(14) Zhang, Y.; Yang, Z.; Yu, Y.; Wen, B.; Liu, Y.; Qiu, M. Tunable Electromagnetic Interference Shielding Ability in a One-Dimensional Bagasse Fiber/Polyaniline Heterostructure. *ACS Appl. Polym. Mater.* **2019**, *1*, 737−745.
(15) Raagulan, K.; Ghim, J.; Braveenth, R.; Chai, K. Y.; Kim, B. M. Improving the EMI Shielding of Graphene Oxide (GNO)-Coated Glass-Fiber-GNO-MA-Grafted Polypropylene (PP) Composites and Nylon 1D-2D Nanocomposite Foams. *RSC Adv.* **2022**, *12*, 15316−15328.
(16) Chen, J. X.; Li, J. W.; Cheng, C. C.; Chiu, C. W. Piezoelectric Property Enhancement of PZT/Poly(vinylidenefluoride-*co*-trifluoroethylene) Hybrid Films for Flexible Piezoelectric Energy Harvesters. *ACS Omega* **2022**, *7*, 793−803.
(17) Li, J.; Li, Y.; Yang, L.; Yin, S. Ti_3C_2Tx/PANI/Liquid Metal Composite Microspheres with 3D Nanoflower Structure: Preparation, Characterization, and Applications in EMI Shielding. *Adv. Mater. Interfaces* **2022**, *9*, No. 2102266.
(18) Maiti, S.; Shrivastava, N. K.; Suin, S.; Khatua, B. B. Polystyrene/MWCNT/Graphite Nanoplate Nanocomposites: Efficient Electromagnetic Interference Shielding Material through Graphite Nanoplate−MWCNT−Graphite Nanoplate Networking. *ACS Appl. Mater. Interfaces* **2013**, *5*, 4712−4724.
(19) Coleman, J.; Khan, U.; Blau, W. J.; Gun'ko, Y. K. Small But Strong: A Review of the Mechanical Properties of Carbon Nanotube−Polymer Composites. *Carbon* **2006**, *44*, 1624−1652.
(20) Sengupta, R.; Bhattacharya, M.; Bandyopadhyay, S.; Bhowmick, A. K. A Review on the Mechanical and Electrical Properties of Graphite and Modified Graphite Reinforced Polymer Composites. *Prog. Polym. Sci.* **2011**, *36*, 638−670.
(21) Bagotia, N.; Choudhary, V.; Sharma, D. K. Synergistic Effect of Graphene/Multiwalled Carbon Nanotube Hybrid Fillers on Mechanical, Electrical and EMI Shielding Properties of Polycarbonate/Ethylene Methyl Acrylate Nanocomposites. *Composites, Part B* **2019**, *159*, 378−388.
(22) Yu, D.; Dai, L. Self-Assembled Graphene/Carbon Nanotube Hybrid Films for Supercapacitors. *J. Phys. Chem. Lett.* **2010**, *1*, 467−470.
(23) Khan, N.; Anwer, A. H.; Ahmad, A.; Sabir, S.; Sevda, S.; Khan, M. Z. Investigation of CNT/PPy-Modified Carbon Paper Electrodes under Anaerobic and Aerobic Conditions for Phenol Bioremediation in Microbial Fuel Cells. *ACS Omega* **2020**, *5*, 471−480.
(24) Jyothibasu, J. P.; Chen, M. Z.; Lee, R. H. Polypyrrole/Carbon Nanotube Freestanding Electrode with Excellent Electrochemical Properties for High-Performance All-Solid-State Supercapacitors. *ACS Omega* **2020**, *5*, 6441−6451.
(25) Pang, A. L.; Arsad, A.; Ahmadipour, M.; Hamzah, A. A.; Zaini, M. A. A.; Mohsin, R. High Efficient Degradation of Organic Dyes by Polypyrrole-Multiwall Carbon Nanotubes Nanocomposites. *Polym. Adv. Technol.* **2022**, *33*, 1402−1411.
(26) Wang, S.; Zhou, Y.; Liu, Y.; Wang, L.; Gao, C. Enhanced Thermoelectric Properties of Polyaniline/Polypyrrole/Carbon Nanotube Ternary Composites by Treatment with a Secondary Dopant Using Ferric Chloride. *J. Mater. Chem. C* **2020**, *8*, 528−535.
(27) Zhang, Z.; Chen, G.; Wang, H.; Zhai, W. Enhanced Thermoelectric Property by the Construction of a Nanocomposite 3D Interconnected Architecture Consisting of Graphene Nanolayers Sandwiched by Polypyrrole Nanowires. *J. Mater. Chem. C* **2015**, *3*, 1649−1654.
(28) Zhu, Q.; Li, E.; Liu, X.; Song, W.; Li, Y.; Wang, X.; Liu, C. Epoxy Coating with In-Situ Synthesis of Polypyrrole Functionalized Graphene Oxide for Enhanced Anticorrosive Performance. *Prog. Org. Coat.* **2020**, *140*, No. 105488.
(29) Seid, L.; Lakhdari, D.; Berkani, M.; Belgherbi, O.; Chouder, D.; Vasseghian, Y.; Lakhdari, N. High-Efficiency Electrochemical Degradation of phenol in Aqueous Solutions Using Ni-PPy and Cu-PPy Composite Materials. *J. Hazard. Mater.* **2022**, *423*, No. 126986.
(30) Gai, S.; Wang, B.; Wang, X.; Zhanga, R.; Miao, S.; Wu, Y. Ultrafast NH_3 Gas Sensor Based on Phthalocyanine-Optimized Non-Covalent Hybrid of Carbon Nanotubes with Pyrrole. *Sens. Actuators, B* **2022**, *357*, No. 131352.
(31) Mo, M.; Zhao, W.; Chen, Z.; Yu, Q.; Zeng, Z.; Wu, X.; Xue, Q. Excellent Tribological and Anti-Corrosion Performance of Polyurethane Composite Coatings Reinforced with Functionalized Graphene and Graphene Oxide Nanosheets. *RSC Adv.* **2015**, *5*, 56486−56497.
(32) Ramôa, S. D.; Barra, G. M.; Oliveira, R. V.; Cossa, M.; Soares, B. G. Electrical, Rheological and Electromagnetic Interference Shielding Properties of Thermoplastic Polyurethane/Carbon Nanotube Composites. *Polym. Int.* **2013**, *62*, 1477−1484.
(33) Jia, P.; Zhu, Y.; Lu, J.; Wang, B.; Song, L.; Wang, B.; Hu, Y. Multifunctional Fireproof Electromagnetic Shielding Polyurethane Films with Thermal Management Performance. *Chem. Eng. J.* **2022**, *439*, No. 135673.
(34) Avadhanam, V.; Thanasamy, D.; Mathad, J. K.; Tumuki, P. Single Walled Carbon Nano Tube-Polyaniline Core-Shell/Polyurethane Polymer Composite for Electromagnetic Interference Shielding. *Polym. Compos.* **2018**, *39*, 4105−4114.
(35) Verma, M.; Chauhan, S. S.; Dhawan, S. K.; Choudhary, V. N. Graphene Nanoplatelets/Carbon Nanotubes/Polyurethane Composites as Efficient Shield Against Electromagnetic Polluting Radiations. *Composites, Part B* **2017**, *120*, 118−127.
(36) Zhou, Y. K.; He, B. L.; Zhou, W. J.; Huang, J.; Li, X. H.; Wu, B.; Li, H. L. Electrochemical Capacitance of Well-Coated Single-Walled Carbon Nanotube with Polyaniline Composites. *Electrochim. Acta* **2004**, *49*, 257−262.
(37) Li, Y.; Liu, J.; Wang, S.; Zhang, L.; Shen, B. Self-Templating Graphene Network Composites by Flame Carbonization for Excellent Electromagnetic Interference Shielding. *Composites, Part B* **2020**, *182*, No. 107615.
(38) Abdah, M. A. A. M.; Razali, N. S. M.; Lim, P. T.; Kulandaivalu, S.; Sulaiman, Y. One-Step Potentiostatic Electrodeposition of Polypyrrole/Graphene Oxide/Multi-Walled Carbon Nanotubes Ternary Nanocomposite for Supercapacitor. *Mater. Chem. Phys.* **2018**, *219*, 120−128.
(39) Armes, S. P. Optimum Reaction Conditions for the Polymerization of Pyrrole by Iron(III) Chloride in Aqueous Solution. *Synth. Met.* **1987**, *20*, 365−371.
(40) Lu, M.; Xie, R.; Liu, Z.; Zhao, Z.; Xu, H.; Mao, Z. Enhancement in Electrical Conductive Property of Polypyrrole-Coated Cotton Fabrics Using Cationic Surfactant. *J. Appl. Polym. Sci.* **2016**, *133*, No. 43601.
(41) Gupta, N. D.; Banerjee, D.; Das, N. S.; Chattopadhyay, K. K. Kinetics of Micelle Formation and their Effect on the Optical and Structural Properties of Polypyrrole Nanoparticles. *Colloids Surf., A* **2011**, *385*, 55−62.
(42) Zhang, X.; Zhang, J.; Wang, R.; Zhu, T.; Liu, Z. Surfactant-Directed Polypyrrole/CNT Nanocables: Synthesis, Characterization, and Enhanced Electrical Properties. *ChemPhysChem* **2004**, *5*, 998−1002.
(43) Xiao, Q.; Wang, P. H.; Ji, L. L.; Tan, X. K.; Ouyang, L. L. Dispersion of Carbon Nanotubes in Aqueous Solution with Cationic Surfactant CTAB. *J. Inorg. Mater.* **2007**, *22*, 1122−1126.
(44) Ramesh, S.; Haldorai, Y.; Kim, H. S.; Kim, J. H. A nanocrystalline Co_3O_4@Polypyrrole/MWCNT Hybrid Nanocompo-

https://doi.org/10.1021/acsomega.2c06613
ACS Omega 2022, 7, 45697−45707

site for High Performance Electrochemical Supercapacitors. *RSC Adv.* **2017**, *7*, 36833−36843.
(45) Wang, Y.; Yang, J.; Wang, L.; Du, K.; Yin, Q.; Yin, Q. Polypyrrole/Graphene/Polyaniline Ternary Nanocomposite with High Thermoelectric Power Factor. *ACS Appl. Mater. Interfaces* **2017**, *9*, 20124−20131.
(46) Baghdadi, N.; Zoromba, M. S.; Abdel-Aziz, M. H.; Al-Hossainy, A. F.; Bassyouni, M.; Salah, N. One-Dimensional Nanocomposites Based on Polypyrrole-Carbon Nanotubes and Their Thermoelectric Performance. *Polymers* **2021**, *13*, No. 278.
(47) Khamlich, S.; Barzegar, F.; Nuru, Z. Y.; Dangbegnon, J. K.; Bello, A.; Ngom, B. D.; Manyala, N.; Maaza, M. Polypyrrole/Graphene Nanocomposite: High Conductivity and Low Percolation Threshold. *Synth. Met.* **2014**, *198*, 101−106.
(48) Wu, T. M.; Lin, S. H. Synthesis, Characterization, and Electrical Properties of Polypyrrole/Multiwalled Carbon Nanotube Composites. *J. Polym. Sci., Part A: Polym. Chem.* **2006**, *44*, 6449−6457.
(49) Tran, X. T.; Park, S. S.; Song, S.; Haider, M. S.; Imran, S. M.; Hussain, M.; Kim, H. T. Electroconductive Performance of Polypyrrole/Reduced Graphene Oxide/Carbon Nanotube Composites Synthesized Via *in Situ* Oxidative Polymerization. *J. Mater. Sci.* **2019**, *54*, 3156−3173.
(50) Lin, W.-D.; Chang, H. M.; Wu, R. J. Applied Novel Sensing Material Graphene/Polypyrrole for Humidity Sensor. *Sens. Actuators, B* **2013**, *181*, 326−331.
(51) Kherroub, D. E.; Bouhadjar, L.; Boucherdoud, A. Synthesis and Characterization of Novel Conductive Copolymer Poly-[(phenylazepane-2-one)-co-(pyrrole)] with Improved Solubility and Conductivity Properties. *J. Mater. Sci.* **2021**, *56*, 1827−1841.
(52) Dhibar, S.; Das, C. K. Silver Nanoparticles Decorated Polypyrrole/Graphene Nanocomposite: A Potential Candidate for Next-Generation Supercapacitor Electrode Material. *J. Appl. Polym. Sci.* **2017**, *134*, No. 44724.
(53) Fan, Y.; Liua, Y.; Cai, Q.; Liu, Y.; Zhang, J. Synthesis of CTAB-Intercalated Graphene/Polypyrrole Nanocomposites Via *in Situ* Oxidative Polymerization. *Synth. Met.* **2012**, *162*, 1815−1821.
(54) Song, W. L.; Cao, M. S.; Lu, M. M.; Bi, S.; Wang, C. Y.; Liu, J.; Yuan, J.; Fan, L. Z. Flexible Graphene/Polymer Composite Films in Sandwich Structures for Effective Electromagnetic Interference Shielding. *Carbon* **2014**, *66*, 67−76.
(55) Saheeda, P.; Jayaleksmi, S. Liquid/Liquid Interfacial Polymerization as an Effective Synthesis Approach for Polypyrrole/MWCNTs Nanocomposite with Impressive Nonlinear Optical Properties. *Opt. Mater.* **2020**, *104*, No. 109940.
(56) Soong, Y. C.; Li, J. W.; Chen, Y. F.; Chen, J. X.; Sanchez, W. A. L.; Tsai, W. Y.; Chou, T. Y.; Cheng, C. C.; Chiu, C. W. Polymer-Assisted Dispersion of Boron Nitride/Graphene in a Thermoplastic Polyurethane Hybrid for Cooled Smart Clothes. *ACS Omega* **2021**, *6*, 28779−28787.
(57) Mikinka, E.; Siwak, M. Recent Advances in Electromagnetic Interference Shielding Properties of Carbon-Fibre-Reinforced Polymer Composites−A Topical Review. *J. Mater. Sci.: Mater. Electron.* **2021**, *32*, 24585−24643.
(58) Shahapurkar, K.; Gelaw, M.; Tirth, V.; Soudagar, M. E. M.; Shahapurkar, P.; Mujtaba, M. A.; Kiran, M. C.; Ahmed, G. M. S. Comprehensive Review on Polymer Composites as Electromagnetic Interference Shielding Materials. *Polym. Polym. Compos.* **2022**, *30*, No. 096739112211021.
(59) Wang, M.; Tang, X. H.; Cai, J. H.; Wu, H.; Shen, J. B.; Guo, S. Y. Fabrication, Mechanism and Prospective of Conductive Polymer Composites with Multiple Interfaces for Electromagnetic Interference Shielding: A Review. *Carbon* **2021**, *177*, 377−402.
(60) He, Z. Z.; Yu, X.; Yang, J. H.; Zhang, N.; Huang, T.; Wang, Y.; Zhou, Z. W. Largely Enhanced Dielectric Properties of Poly(Vinylidene Fluoride) Composites Achieved by Adding Polypyrrole-Decorated Graphene Oxide. *Composites, Part A* **2018**, *104*, 89−100.
(61) Hu, W.; Zhang, J.; Liu, B.; Zhang, C.; Zhao, Q.; Sun, Z.; Cao, H.; Zhu, G. Synergism Between Lignin, Functionalized Carbon Nanotubes and Fe_3O_4 Nanoparticles for Electromagnetic Shielding Effectiveness of Tough Lignin-Based Polyurethane. *Compos. Commun.* **2021**, *24*, No. 100616.
(62) Gahlout, P.; Choudhary, V. EMI Shielding Response of Polypyrrole-MWCNT/Polyurethane Composites. *Synth. Met.* **2020**, *266*, No. 116414.
(63) Omana, L.; Chandran, A.; John, R. E.; Wilson, R.; George, K. C.; Unnikrishnan, N. V.; Varghese, S. S.; George, G.; Simon, S. M.; Paul, I. Recent Advances in Polymer Nanocomposites for Electromagnetic Interference Shielding: A Review. *ACS Omega* **2022**, *7*, 25921−25947.

https://doi.org/10.1021/acsomega.2c06613
ACS Omega 2022, 7, 45697−45707